Registration to a neuroanatomical reference atlas - identifying glomeruli in optical recordings of the honeybee brain.

Martin Strauch[1*] , C. Giovanni Galizia[1]
1: Department for Neurobiology, University of Konstanz, Germany
*: Martin.Strauch@uni-konstanz.de

Abstract: An odorant stimulus given to a bee elicits a characteristic combinatorial pattern of activity in neuronal units called glomeruli. These patterns can be measured by optical imaging, however detecting and identifying the glomeruli is a laborious task and prone to errors. Here, we present an image analysis pipeline for the automatic detection and identification of glomeruli. It involves Independent Component Analysis (ICA) to detect glomeruli in CCD camera data, a filtering step to exclude non-glomerulus objects and a graph-matching approach to find the best projection of the observed brain region onto a reference atlas. We evaluate our method against a manual glomerulus identification performed by a human expert and show that we achieve reliable results. Employing our method, we are now able to screen multiple recordings with the same accuracy, yielding a homogeneous collection of glomerulus identity mappings. These will subsequently be used to extract activity patterns that can be compared between individuals.

1 Introduction

The olfactory sense of insects is a popular model for studies on signal perception, learning and memory formation. It is not only of biological interest, but given an insect's remarkable performance in discrimination, as well as generalisation of chemicals, unveiling the principles behind insect olfaction could also be important for chemoinformatics or classification algorithms in general [LD06, GSSG05].

Briefly, information about odorants is generated by receptor cells, each of which has a certain receptive range, i.e. responds to several chemicals with varying strength. The honeybee *Apis mellifera* has tens of thousands of receptor cells, but only 160 different types of receptors. It is in the antennal lobe (AL), the first instance of olfactory information processing in the insect brain, that the information from all these receptors is assembled, forming a code word that depends on the input odorants, their relative proportion and overall concentration.
The olfactory code is based on glomeruli, lumps of coherently acting neurites in the AL, as basic units of information. Each of them receives input from one of the 160 receptor types (in the honeybee; numbers vary between species). Together, they form a combinatorial code, each input generating a characteristic pattern of glomerulus activity, i.e. code word, which is conserved for all members of a species [GM00, GSRM99].

In calcium-imaging experiments, a calcium-sensitive fluorescent dye is used to report changes in intracellular calcium concentration, which is indicative of neuronal activity. Thus, using a CCD camera to record changes in fluorescent light intensity, we are able to monitor glomerulus activity patterns in response to defined input odorants. For details on the experimental technique please refer to [SG02, GV04].

Any evaluation of glomerular activity patterns across individuals requires an accurate glomerulus identification. As no rigorous method has been proposed for this task as of today (see [SG02, GV04] for previous, manual approaches) , we present here a method for the automatic detection and subsequent identification, i.e. labelling, of glomeruli in the honeybee antennal lobe.

First, we need to detect glomeruli in CCD camera data, i.e. find the pixels which together constitute a glomerulus. We therefore employ Independent Component Analysis [HO00] to detect pixels that change coherently in front of a random background, allowing us to compile a map of the objects observed during the experiment (section 2.1). We then denoise the map and apply a shape-filter based on anatomical criteria to exclude objects that are not glomeruli (section 2.2).

The identification of the glomeruli then amounts to a registration of the glomerulus map to the 3D reference atlas of the honeybee AL [GMM99] where glomeruli are assigned unique labels. Previously, the identification of glomeruli has been a laborious task for human experts, prone to variations in accuracy. A 2D view of the AL as provided by the camera recordings has to be projected onto the 3D atlas, a task that is complicated by experimental noise and biological variability that often leads to changes in glomerulus position in individual bees. Moreover, several of the glomeruli present in a slice from the atlas may not be visible in the actual data, as they do not respond to any of the tested odorants or because they accidentally remained unstained during the experiment.

In order to identify the glomeruli, we transform both the map and the 3D atlas into adjacency graphs with glomeruli as nodes (section 2.3). Using an exact *Branch&Bound* approach for graph matching, we find the projection of the 2D map onto the 3D atlas which comes closest to representing a subgraph isomorphism. Due to the aforementioned biological variability, an exact isomorphism may not always exist. We account for this variability by scoring the graphs according to a penalty matrix for deviations from the atlas geometry.
The matching we perform is related to *subgraph isomorphism*, which is known to be NP-complete [GJ90]. Thus, a complete search that takes all possible combinations of node projections and positional variations into account will be time-consuming. In practice, however, graphs are moderately sized and *a priori* knowledge is often available that helps to efficiently speed up the search process (see section 2.3).

For evaluation, we compare our method to a ”ground truth” on a dataset manually examined by a human expert and find that it achieves reliable results (section 3). Given the deterministic nature of the graph-matching algorithm, we suggest that it is better suited for an integrative analysis of multiple datasets than different manual, often undocumented, algorithms performed by the respective experimentators.

2 Materials and Methods

2.1 Detecting glomeruli with ICA

Independent Component Analysis (ICA) is a method for feature extraction and blind source separation [HO00]. ICA has already found applications in neuroscience, e.g. in the fields of EEG and MEG recording analysis, where it is used to separate the actual signals of interest from artifacts such as muscle or eye activity [VSJ$^+$00].
In the ICA paradigm it is assumed that a number of observers record several independent signals, which, due to the recording situation, can occur to them as mixtures and may be obscured by noise. While in the EEG application the focus was on the different temporal contributions of each component, we are interested in spatial components that change their activity coherently over time. Here, the independent signals correspond to glomeruli: each glomerulus sends a signal, i.e. its state of activation, which is obscured by experimental noise. Additionally, signal superposition may occur in some cases if glomeruli lie on top of each other.
The task for the ICA is to separate signals from noise and thus to detect glomeruli. We interpret all the pixels of the CCD camera recording as observers $\mathbf{x}(t)$, which, at time instant t, perceive n signals $(s_1(t), \ \dots \ , s_n(t))$ that are transformed by vectors $(\mathbf{a}_1, \ \dots \ , \mathbf{a}_n)$, which can, in an abstract sense, be regarded as the parameters of the recording situation, e.g. properties of the dye, the camera etc. The number of glomeruli may be smaller than n, as other objects can also generate signals.

$$\mathbf{x}(t) = \sum_{i=1}^{n} \mathbf{a}_i s_i(t) = \mathbf{A}\mathbf{s}(t) \tag{1}$$

The ICA problem is to estimate the source signals and the coefficients of the so-called mixing matrix $\mathbf{A}$ based on the (ideal) assumption that the signals are statistically independent and non-gaussian. In practice, however, the strict independence requirement may be relaxed.
In our case, pixels belonging to the same glomerulus will be considered as carrying the same signal $s_i(t)$. Two pixels from different glomeruli will display different behaviour over time and they will be associated with two different signal components $s_i(t)$ and $s_j(t)$.

While exact solutions to the ICA problem are computationally expensive, several efficient algorithms for approximate solutions are available, e.g. the popular *fastICA* algorithm [HO00]. We implemented our approach in Java, employing the open-access platform KNIME (*www.knime.org*) that supports data exchange with R (*www.r-project.org*) . For the ICA we could thus make use of the R-package *fastICA* [MHR07] that implements the mentioned ICA algorithm.

We found that 2000 iterations of *fastICA* were sufficient to obtain stable, reproducible results. We set the number of expected independent components to 50, which is greater than the number of about 20-30 glomeruli that is commonly found in one 2D view of the antennal lobe. This is to account for the fact that other, non-glomerulus structures are often accidentally stained with the fluorescent dye, giving rise to artifact signals that are

separated out by the ICA as further independent components. A subsequent filtering step (see section 2.2) was employed to tell apart glomeruli and other objects.

Each independent component identified by the ICA resulted in an image with the dimensions of the original video data with one glomerulus (or other object) enhanced but not yet neatly cut out (see inlay in *Figure 2b*). For construction of the glomerulus map, we thus separated signal and residual noise in each of these images by regarding only those pixels as signal, whose values were above the upper whisker ($1.5 \times$ IQR above the 3rd quartile) of the box-plot of all pixel values in the image. Overlaying and false-coloring all components we then could construct a glomerulus map of the observed part of the AL (*Figure 2b*).

2.2 Filtering

As previously mentioned, objects other than glomeruli can also appear in the recordings. As this complicates the identification, we thus aimed at cleaning up the map such that only glomeruli remain. For this step, we employed two anatomically motivated criteria, namely object size and circularity. Glomeruli are relatively large, more or less globular objects. In the two space dimensions of calcium-imaging recordings they appear to be roughly circular. Non-glomerulus structures, on the other hand, result e.g. from experimental noise, yielding smaller, scattered objects or may be parts of trachees or the antennal nerve, which are rather elongated structures.
For the filtering we thus demanded a minimum size, i.e. a threshold t_p denoting the number of contiguous pixels. Circularity was measured by drawing a circle around the object's centroid. The radius was set to half the longest diameter of the object. The degree of circularity $degree_c$ was then measured as the ratio

$$degree_c = \frac{\#\text{ pixels (object)}}{\#\text{ pixels (circle)}} \tag{2}$$

For the data analysed in this study we set the default parameters to $t_p = 50$ pixels and the circularity threshold $t_{degree_c} = 0.6$. For objects with more than 3 neighbours we reduced the circularity threshold to $\frac{1}{2}\ t_{degree_c}$ to account for the fact that in dense regions of the recording glomeruli actually lie on top of each other, thus obscuring parts of the circular shape.
Filtering by size also results in de-noising as a side-effect. While the circularity threshold reflects mainly biological proportions, t_p is more dependent on the resolution of the recording and needs to be adjusted for other datasets. As there is variation between individuals, we had to lower both thresholds ($t_p = 40$ and $t_{degree_c} = 0.5$) for some animals in order not to discard glomeruli. To automatise this step, one could define thresholds relative to the average size and circularity of objects in the recording.

2.3 Registration to the atlas with graph-matching

We transformed the previously constructed AL map into a topological graph $S = (V_S, E_S)$ with glomeruli as the set of nodes V_S. Edges E_S between two nodes were drawn if the respective glomeruli touched each other. Edges were annotated with the relative position of the glomeruli's centroids to each other based on the angle between them on a polar grid (see *Figure 1a*). We allowed 8 categories of positional information, i.e. $0°$, $45°$, ... $315°$.

The same positional annotation applied for the atlas graph $G = (V_G, E_G)$ which was based on the topological information contained in the reference atlas of the honeybee AL [GMM99]. Taking into account that the 2D view of the AL represents not a perfect 2D slice but rather the focal plane that may also contain glomeruli from above and below, we accepted also glomeruli touching on the z-axis as neighbouring. For edge annotation, however, we used the same 8 categories of 2D positional information, neglecting the position on the z-axis.
Additionally, a systematical source of variation was taken into account: all members of one of the rosetta-like glomerulus clusters in the atlas, were also regarded as neighbours. Some of these glomeruli appear actually distant in the atlas, but may frequently collapse onto each other in case this is not prevented by solid obstacles such as other glomeruli or structural elements in the AL. These anatomical variations are discussed in [GMM99]. We consequently chose to connect the members of these clusters by edges, but marked them as facultative edges.

Including these rules we ensured that the set of atlas graph edges always remains a superset of the set of map graph edges: $E_S \subseteq E_G$. Having more edges in the atlas graph than expected based on biological knowledge, we could consider every edge from E_S which was also in E_G to be consistent with the atlas topology. Conversely, every edge from E_S which was not in E_G was regarded as a violation of the atlas topology.

We employed a topological score to measure for a candidate subgraph S' the consistency of its edge set $E_{S'}$ with the atlas edge set E_G. A scoring or penalty matrix (*Figure 1b*) was used as a parameter for the amount of biological variation that should be allowed. Slight deviations from the atlas topology received only slight penalties ($p = 0.25$), whereas gross violations of the atlas topology, such as a mismatch $E_{S'} \ni E' : \ 0° \ , \ E_G \ni E : \ 180°$ received a larger penalty ($p = 1$). Facultative edges were allowed but at an additional cost of $p = 0.25$. The scoring matrix can be regarded as a parameter specifying the variability of glomerulus positions in the honeybee AL. For other species, different parameter settings may apply.

Having defined the scoring matrix, we could search for an isomorphic or close to isomorphic projection of the map subgraph onto the atlas graph, taking a low overall score (the sum of the individual edge scores) as indicative of a good match.
Using a depth-first *Branch&Bound* search strategy, we chose a seed node from the map graph and subsequently assigned all atlas nodes to it, at each step computing all possible assignments of children nodes of the two nodes to each other. All of these assignments were scored and followed on iteratively if the current partial score did not exceed the

overall minimum score for a complete projection and if no gross violation, i.e. $p \geq 1$ occurred. The latter helped to identify obvious orientation mismatches at an early stage.

Using the above search strategy, we were able to efficiently enumerate all valid (with no $p \geq 1$ for any node; consistent node assignments, e.g. no atlas graph node assigned twice) projections. In practice, we kept all valid projections in a search tree and scored all possible paths through the tree, starting at the root, identifying the least scoring path as the desired best approximation to an isomorphism.
The approach described above works without any additional information. However, in order to reduce the number of isomorphic solutions we made use of *a priori* knowledge in the form of a marker glomerulus. Chemical substances such as nonanol can be employed as markers as they elicit a characteristic response, activating one glomerulus - the marker glomerulus - far more than the others in the observed region of the AL. In these cases, we thus knew the correct projection of one of the nodes *a priori*. Hence, we could introduce a constraint to better tell apart solutions with similar scores. Additionally, this provides an excellent seed for the above graph matching approach.

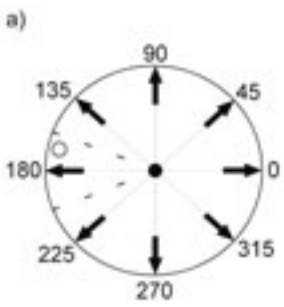

b)

atlas

map	∉	↑	↓	←	→	↖	↘	↗	↙
∉	0	0	0	0	0	0	0	0	0
↑	1	0	1	0.75	0.75	0.25	1	0.25	1
↓	1	1	0	0.75	0.75	1	0.25	1	0.25
←	1	0.75	0.75	0	1	0.25	1	1	0.25
→	1	0.75	0.75	1	0	1	0.25	0.25	1
↖	1	0.25	1	0.25	1	0	1	0.75	0.75
↗	1	1	0.25	1	0.25	1	0	0.75	0.75
↘	1	0.25	1	1	0.25	0.75	0.75	0	1
↙	1	1	0.25	0.25	1	0.75	0.75	1	0

Figure 1: a) Topological coding: The edge between the black and the white node is annotated with 180° ($\leftarrow$). b) Penalty (scoring) matrix defining the penalty for mismatches between edge annotation in the atlas graph and the map subgraph. If an edge exists in the map (e.g. $\uparrow$), but not in the atlas ($\notin$), this results in a high penalty of $p = 1$. Slight positional variabilities are given lower penalties. As we assume $E_S \subseteq E_G$, atlas edges are allowed to be missing in the map ($p = 0$, see first row).

2.4 Dataset used in this study

The dataset used for the evaluation of our method was taken from [Dit05]. Bee preparation and staining with the calcium-sensitive fluorescent dye fura-dextran were performed as described in [SG02]. Monochromatic light was used for the excitation of the dye. For each odorant measured, two times 40 images (two sequential, quasi-simultaneous images for 340 nm and 380 nm) were taken at a frequency of 5 Hz and a spatial resolution of 2×2 μm per pixel using a TillPhotonics CCD camera and an Olympus BX50WI microscope fitted with a $20\times$ objective lens (TillPhotonics, Germany; Olympus, Germany).
The images contained in the evaluation dataset were constructed using the pixel-wise ratio

of the 340 nm and 380 nm images. The resolution of the images was 160×120 pixels. 16 aliphatic hydrocarbons at 4 different concentrations (10^{-1} to 10^{-4} dilution in mineral oil) were used as odorants. The odorants were presented to the bees from image 11 to 15 of the 40 images recorded.
For glomerulus detection, we concatenated all 40-image recordings that were done in the same animal in order to see as many glomeruli active as possible. Depending on the number of odorant responses measured, this amounted to between 600 and 1200 images per animal. Manual detection and identification of glomeruli was performed as described in [Dit05] using the honeybee AL reference atlas and one marker glomerulus.

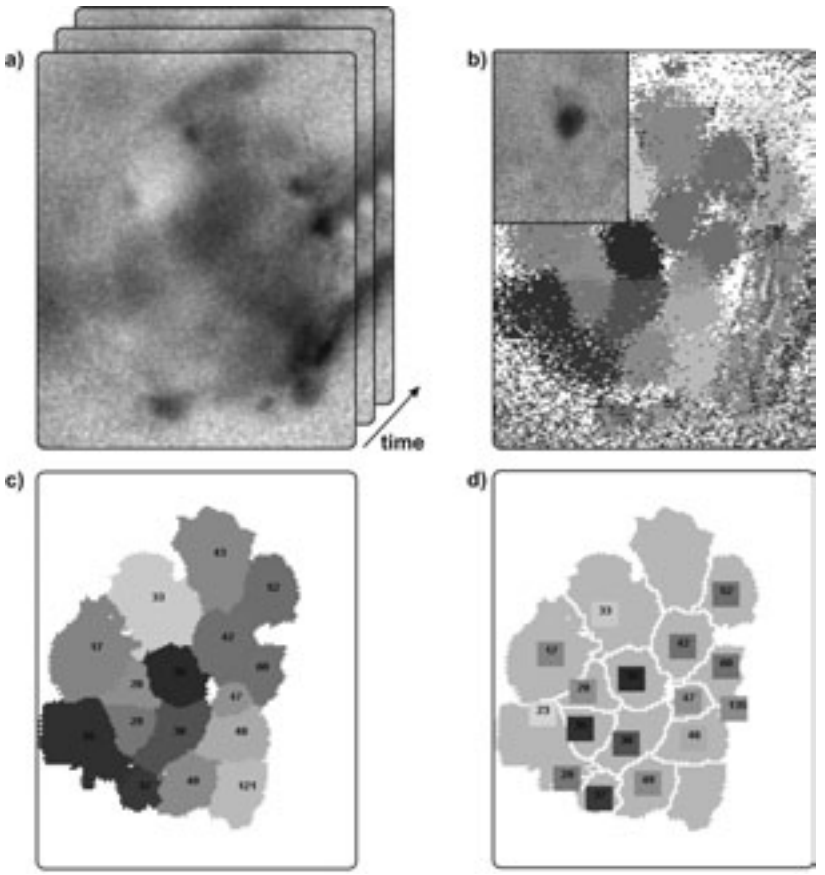

Figure 2: ICA is performed on camera recordings (animal 12) (a) to obtain a map of the AL (b). The inlay in b) shows one of the independent components that were used to construct the map. Through filtering, non-glomerulus objects are discarded. A graph-matching approach identifies the glomeruli, resulting in a labelled AL map (c). For comparison, a human expert labelling is shown (d).

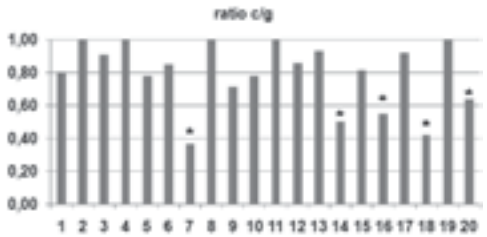

Figure 3: Performance for 20 different animals. The bars represent the ratio $\frac{c}{g}$, where c is the number of glomeruli which received a common label in both the manual and the computed solution, while g stands for the total number of glomeruli.

3 Results

We produced labelled AL maps for a dataset consisting of 20 different animals. An example showing the individual processing steps of our method is given in *Figure 2*. Reproducibility of the maps was generally high. For each animal, 10 runs of the ICA and subsequent filtering were performed to generate 10 maps per animal. The average pairwise pixel overlap between the maps from the same animal was 94%. Deformations of individual glomeruli occurred, the overall map layout, however, was always the same.

To assess the quality of our glomerulus identification, we evaluated the overlap of the computed and the hand-made labelling. The hand-made labellings [Dit05] provided us with coordinates of glomerulus centroids as the human expert saw them (no shape information was recorded). We placed the centroids onto the corresponding maps (see *Figure 2d)* and counted all matches, i.e. positions where both our computed maps and the hand-made labelling agreed on having detected a glomerulus. We defined this as the number of glomeruli g that were visible in the respective AL. Cases like glomeruli 43/121 and 135 which exist only in one of the maps (*Figure 2c/d*) did not influence g.

In order to evaluate the performance of our method we computed the ratio $\frac{c}{g}$, where c is the number of glomerulus labels both maps had in common. Thus, two labellings perfectly in accordance with each other resulted in a ratio of 1.
On average, we achieved a ratio of 0.79 with 5 labellings being 100 percent correct (see *Figure 3*). A typical example is shown in *Figure 2c*, where 14 glomeruli were detected by both the computational and the manual approach. Here, 12 glomeruli received the same label, resulting in a ratio of 0.86. In this example, the source of disagreement between manual and computed solution is the different perception of glomerulus 35 (computed) which was identified as two glomeruli (23 and 29) by the manual approach.

Typically, minor disagreements on the identity of a single glomerulus occured in the outer regions of the maps, where glomeruli have less neighbours and thus less geometrical constraints, giving rise to multiple solutions of equal or similar probability. When ratios were below 0.6, this was the result of follow-on mistakes: if a glomerulus more towards

the middle of the map received a wrong label, adjacent glomeruli were consequently shifted compared to the manual solution, which explains the relatively high number of disagreements in those cases (marked with * in *Figure 3*). These solutions received, however, slightly better scores than the correct solution. Post-hoc human identification clarified that in all of these cases the computed solution was also compliant with the reference atlas. In order to resolve this, one would need a new marker, i.e. another constraint in a different region of the AL to further reduce the number of similarly scoring projections.

Computing time for the graph matching differed depending on the number of glomeruli visible in a particular 2D view of the AL (minimum 5, maximum 20, median 12) and the uniqueness of the correct solution. In case of many equally well scoring projections, all of them had to be followed deep into the search tree, preventing an early bound. On a 4 CPU machine ($4\times$ Intel® Xeon® 2.33 GHz), computing time for the data described in this work was in a range between below one second up to about 13 minutes. The ICA took on average 3-4 minutes on a desktop computer.

4 Conclusion

We have proposed an image analysis method for the detection and identification of glomeruli in the honeybee AL. The average accuracy of its results lies well in the range of human performance, however in some cases the best score according to the given scoring matrix did not correspond to the projection chosen by the human expert. These results leave room for future optimisations of the parameters, i.e. the connectivity of the atlas graph and the scoring matrix. Both reflect biological properties, i.e. anatomy and anatomical variability and could be learned from training data.
Further, we accepted the manual glomerulus identification as a ground truth for evaluation purposes. Although the manual identification was performed very carefully, errors may nevertheless have occurred. The manual identification is usually very reliable close to the marker glomerulus (17 or 33 in this dataset), however accuracy decreases with increasing distance from the fixed point indicated by the marker.
In order to improve the quality of glomerulus identification, both manual and computational, it may thus be necessary to use multiple marker glomeruli to cover the relevant parts of the AL.

Computation time is generally unproblematic, however it could become an issue for real-time application of the method while the experiment is running and for datasets where more glomeruli are visible. Future improvements could also involve extensive preprocessing of the atlas graph, making use of the fact that it does not change between the experiments. This would allow for polynomial time subgraph matching against the preprocessed atlas graph, however at the cost of increasing space requirements [MB99].

In summary, we have devised a method that allows to deterministically identify glomeruli in calcium-imaging recordings of the honeybee AL. By employing a penalty matrix for deviations from the atlas geometry we have introduced a rigorous definition of a good

registration fit to replace hand-made glomerulus labellings. Our graph-matching approach allows to automatically search for the optimal solution based on the score criterion.

With the image analysis pipeline at hand it now becomes possible to screen multiple datasets with the same accuracy. Glomerular activation patterns from different studies can be combined to build a data pool that will subsequently be used as a resource for data mining approaches aimed at understanding information processing in insect brains.

5 Acknowledgements

We thank Mathias Ditzen for offering us his dataset and the results of the manual glomerulus identification [Dit05]. We also acknowledge helpful discussions with Michael Berthold and Julia Rein. This work was supported by the German Ministry for Education and Science (BMBF grant 576/07) and partially supported by the DFG Research Training Group GK-1042 "Explorative Analysis and Visualization of Large Information Spaces".

References

[Dit05] M. Ditzen. *Odor concentration and identity coding in the antennal lobe of the honeybee Apis mellifera*. PhD thesis, Freie Universität Berlin, URL: http://www.diss.fu-berlin.de/2005/211/indexe.html, 2005.

[GJ90] M.R. Garey and D.S. Johnson. *Computers and Intractability; A Guide to the Theory of NP-Completeness*. W. H. Freeman & Co., New York, NY, USA, 1990.

[GM00] C.G. Galizia and R. Menzel. Odour perception in honeybees: coding information in glomerular patterns. *Curr Opin Neurobiol*, 10(4):504–510, Aug 2000.

[GMM99] C.G. Galizia, S.L. McIlwrath, and R. Menzel. A digital three-dimensional atlas of the honeybee antennal lobe based on optical sections acquired by confocal microscopy. *Cell Tissue Res*, 295(3):383–394, Mar 1999.

[GSRM99] C.G. Galizia, S. Sachse, A. Rappert, and R. Menzel. The glomerular code for odor representation is species specific in the honeybee Apis mellifera. *Nat Neurosci*, 2(5):473–478, May 1999.

[GSSG05] F. Guerrieri, M. Schubert, J.C. Sandoz, and M. Giurfa. Perceptual and neural olfactory similarity in honeybees. *PLoS Biol*, 3(4):e60, Apr 2005.

[GV04] C. G. Galizia and R.S. Vetter. *Chapter 13 in "Advances in Insect Sensory Neuroscience" (ed. T.A. Christensen)*, pages 349–392. CRC Press, Boca Raton, 2004.

[HO00] A. Hyvärinen and E. Oja. Independent component analysis: algorithms and applications. *Neural Networks*, 13(4-5):411–430, 2000.

[LD06] X. Liu and R.L. Davis. Insect olfactory memory in time and space. *Curr Opin Neurobiol*, 16(6):679–685, Dec 2006.

[MB99] B.T. Messmer and H. Bunke. A decision tree approach to graph and subgraph isomorphism detection. *Pattern Recognition*, 32(12):1979–1998, Dec 1999.

[MHR07] J.L. Marchini, C. Heaton, and B.D. Ripley. *fastICA: FastICA Algorithms to perform ICA and Projection Pursuit, version 1.1-8*, Oct 2007.

[SG02] S. Sachse and C.G. Galizia. Role of inhibition for temporal and spatial odor representation in olfactory output neurons: a calcium imaging study. *J Neurophysiol*, 87(2):1106–1117, Feb 2002.

[VSJ+00] R. Vigário, J. Särelä, V. Jousmäki, M. Hämäläinen, and E. Oja. Independent component approach to the analysis of EEG and MEG recordings. *IEEE Trans Biomed Eng*, 47(5):589–593, May 2000.